# Supporting Information for

## Surface plasmon polariton amplification upon electrical injection in highly-integrated plasmonic circuits

*Dmitry Yu. Fedyanin,*[1,*] *Alexey V. Krasavin,*[2] *Aleksey V. Arsenin,*[1] *Anatoly V. Zayats*[2]

[1]Laboratory of Nanooptics and Femtosecond Electronics, Department of General Physics, Moscow Institute of Physics and Technology (State University), 9 Institutsky Lane, Dolgoprudny 141700, Russian Federation

[2]Nano-optics and Near-field Spectroscopy Group, Department of Physics, King's College London, Strand, London WC2R 2LS, United Kingdom

**Numerical simulation of surface plasmon polariton (SPP) amplification**

Carrier flow in the structure is predominantly directed along the *y* axis (Figure S1) and, consequently, one-dimensional electronic simulations are appropriate for description of the proposed amplification scheme.[1]

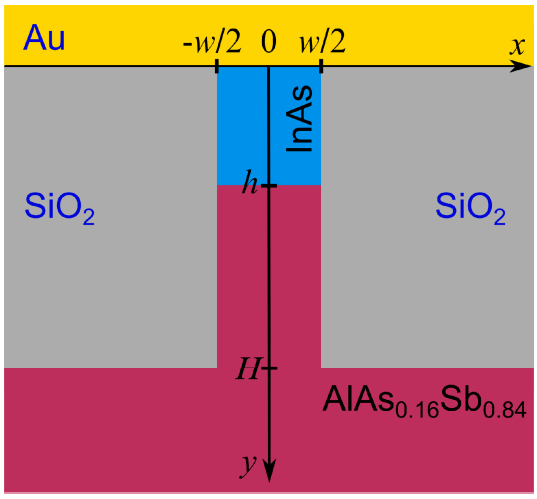


**Figure S1.** Transverse cross-section of the T-shaped waveguide under consideration.

Therefore, the carrier behavior within the semiconductors is described six first order non-linear differential equations

$$\begin{cases} \dfrac{d\varphi}{dy} = -E_y, \\ \dfrac{dE_y}{dy} = \dfrac{4\pi e}{\varepsilon}\left(p - n + N_{\mathrm{d}} - N_{\mathrm{a}}\right), \\ \dfrac{dn}{dy} = \dfrac{1}{eD_{\mathrm{n}}} J_{\mathrm{n}} - \dfrac{\mu_{\mathrm{n}} n}{D_{\mathrm{n}}} E_y, \\ \dfrac{dp}{dy} = -\dfrac{1}{eD_{\mathrm{p}}} J_{\mathrm{p}} + \dfrac{\mu_{\mathrm{p}} p}{D_{\mathrm{p}}} E_y, \\ \dfrac{dJ_{\mathrm{n}}}{dy} = eU = e\left(U_{\mathrm{stim}} + U_{\mathrm{spont}} + U_{\mathrm{Auger}}\right), \\ \dfrac{dJ_{\mathrm{p}}}{dy} = -eU = -e\left(U_{\mathrm{stim}} + U_{\mathrm{spont}} + U_{\mathrm{Auger}}\right), \end{cases} \tag{s1}$$

which are solved using the finite difference method. Here all notations have their usual meaning,[2] i.e. $\varphi$ is the electrostatic potential; $E_y$ is the electric field; $e$ is the electron charge; $\varepsilon$ is the static dielectric constant; $p$ and $n$ are the concentrations of holes and electrons, respectively; $N_{\mathrm{d}}$ and $N_{\mathrm{a}}$ are the donor and acceptor impurity concentrations; $D_{\mathrm{p}}$ and $D_{\mathrm{n}}$, $\mu_{\mathrm{p}}$ and $\mu_{\mathrm{n}}$ are the diffusion coefficients and mobilities for holes and electrons, respectively; $J_{\mathrm{p}}$ and $J_{\mathrm{e}}$ are the hole and electron current densities; $U$ is the electron-hole recombination rate that includes the stimulated emission ($U_{\mathrm{stim}}$), spontaneous emission ($U_{\mathrm{spont}}$) and non-radiative Auger ($U_{\mathrm{Auger}}$) recombination rates. The contribution terms used in the present study are expressed as follows:

$$U_{\mathrm{spont}} = F_{\mathrm{sp}} B(np - n_{\mathrm{eq}} p_{\mathrm{eq}}), \tag{s2}$$

$$U_{\mathrm{Auger}} = \left(C_{\mathrm{p}} p + C_{\mathrm{n}} n\right) \times \left(np - n_{\mathrm{eq}} p_{\mathrm{eq}}\right), \tag{s3}$$

$$U_{\mathrm{stim}} = g P_z / \hbar\omega, \tag{s4}$$

where $n$ and $p$ are the electron and hole concentrations, $n_{\mathrm{eq}}$ and $p_{\mathrm{eq}}$ are the equilibrium electron and hole concentrations, $B$ is the radiative recombination coefficient, $C_{\mathrm{n}}$ and $C_{\mathrm{p}}$ are the electron and hole Auger recombination coefficients, $\omega$ is the SPP frequency, $g$ is the local optical gain, $F_{\mathrm{sp}}$ and $P_z$ are the normalized Purcell factor and power density given by

$$F_{\mathrm{sp}}(y) = \frac{1}{w} \int_{-w/2}^{w/2} F_{\mathrm{p}}(x, y) dx, \tag{s5}$$

$$F_{\mathrm{p}}(x, y) = 1 + \frac{c^3 \left|E(x, y)\right|^2}{4\overline{n}(x, y)\omega^2 \upsilon_{\mathrm{g}} \int_{-\infty-\infty}^{+\infty+\infty} \frac{1}{16\pi} \left(\xi(\tilde{x}, \tilde{y}) \left|E(\tilde{x}, \tilde{y})\right|^2 + \left|H(\tilde{x}, \tilde{y})\right|^2\right) d\tilde{x} d\tilde{y}}, \tag{s6}$$

$$P_z(y) = \frac{1}{w} \int_{-w/2}^{w/2} S_z(x, y) dx. \tag{s7}$$

In the above expressions, $S_z(x,y)$ is the projection of the Poynting vector on the $z$ axis taken from the eigenmode optical simulations (as described in the main text), $\bar{n}(x,y)$ is the real part of the refractive index, $v_g$ is the SPP group velocity, $E(x,y)$ and $H(x,y)$ are the complex electric and magnetic fields of the SPP found in the eigenmode optical simulations, $\xi(x,y)$ is equal to $\bar{n}(x,y)^2$ in the semiconductors and $SiO_2$, while in the metal $\xi(x,y)=1+\omega_p^2/\left(\omega^2+\Gamma^2\right)$, found from the complex dielectric function of the metal calculated using the Drude model $\varepsilon(\omega)=1-\omega_p^2/\left(\omega^2+i\Gamma\omega\right)$ (see section "Calculation of the dielectric function of gold" below). Optical gain connected with band-to-band transitions is given as[4]

$$g(n,p)=g\left(n(F_e),p(F_h)\right)=g(F_e,F_h)=\frac{4\pi^2e^2}{c\bar{n}m_{e0}^2\omega}\left|M_b\right|^2\int_{-\infty}^{+\infty}\left|M_{env}(E,E-\hbar\omega)\right|^2\rho_c(E-E_c)$$
$$\times\rho_v(E_v-E+\hbar\omega)\left[\frac{1}{1+\exp\left((E-F_e)/k_BT\right)}-\frac{1}{1+\exp\left((E-\hbar\omega-F_h)/k_BT\right)}\right]dE, \quad \text{(s8)}$$

where $m_{e0}$ is the free-electron mass, $F_e$ and $F_h$ are the quasi-Fermi levels for electrons and holes, $\bar{n}$ is the real part of the refractive index of the semiconductor, $M_b$ is the average matrix element connecting Bloch states near the band edges and finally $\rho_c$ ($\rho_v$) is the density of states in the conduction (valence) band and $M_{env}$ is the envelope matrix element, both are calculated using Stern's approach.[5,6] In order to use the expression for the optical gain in the finite difference solver, we fit Eq. s8 with a linear function

$$g(n,p)\approx g_{1N}\left[\min(n,p)-N_{tr}\right]. \quad \text{(s9)}$$

In the case of InAs under consideration,[3] $g_{1N}=1.41\times10^{-14}$ cm$^2$ and $N_{tr}=5.0\times10^{14}$ cm$^{-3}$. Band-to-band transitions in $AlAs_{0.16}Sb_{0.84}$ are neglected, since the SPP energy is much less than the bandgap energy of $AlAs_{0.16}Sb_{0.84}$ (1.77 eV).

To complete the model, 12 interface boundary conditions are implemented: three – at the metal-semiconductor contact ($y$=0), six – at the InAs/$AlAs_{0.16}Sb_{0.84}$ heterojunction ($y$=$h$) and three – at the back contact ($y$=$H$). In accordance with the thermionic emission theory, boundary conditions at $y$=0 (Schottky contact) can be written as[2,7]

$$\begin{cases}\varphi\big|_{y=+0}=\phi_b-E_g,\\ J_n\big|_{y=+0}=e\upsilon_{nr}(n\big|_{y=+0}-n_0),\\ J_p\big|_{y=+0}=-e\upsilon_{pr}(p\big|_{y=+0}-p_0),\end{cases} \quad \text{(s10)}$$

where $n_0=N_c^{InAs}F_{1/2}\left((\phi_b-E_g)/k_BT\right)$ and $p_0=N_v^{InAs}F_{1/2}\left(-\phi_b/k_BT\right)$ are the quasi-equilibrium electron and hole concentrations at $y$=0 ($F_{1/2}$ is the Fermi-Dirac integral, $\phi_b$ is the Schottky barrier height for holes, $N_c^{InAs}$ and $N_v^{InAs}$ are the effective densities of states in the conduction and valence bands of InAs), $\upsilon_{nr}$ and $\upsilon_{pr}$ are the effective recombination or collection velocities for electrons and holes, respectively.

At the InAs/$AlAs_{0.16}Sb_{0.84}$ heterojunction, again, the thermionic emission boundary conditions[8,9] are used:

$$\begin{cases} \varphi|_{y=h-0} = \varphi|_{y=h+0}, \\ \varepsilon^{\mathrm{InAs}} E_y|_{y=h-0} = \varepsilon^{\mathrm{AlAs0.16Sb0.84}} E_y|_{y=h+0}, \\ J_{\mathrm{n}}|_{y=h-0} = J_{\mathrm{n}}|_{y=h+0}, \\ J_{\mathrm{n}}|_{y=h+0} = e\upsilon_{\mathrm{nr}}^{\mathrm{AlAs0.16Sb0.84}} n|_{y=h+0} - \dfrac{m_{\mathrm{e}}^{\mathrm{AlAs0.16Sb0.84}}}{m_{\mathrm{e}}^{\mathrm{InAs}}} e\upsilon_{\mathrm{nr}}^{\mathrm{InAs}} \exp\left(-\dfrac{\Delta E_{\mathrm{c}}}{k_{\mathrm{B}}T}\right) n|_{y=h-0}, \\ J_{\mathrm{p}}|_{y=h-0} = J_{\mathrm{p}}|_{y=h+0}, \\ J_{\mathrm{p}}|_{y=h+0} = -e\upsilon_{\mathrm{pr}}^{\mathrm{AlAs0.16Sb0.84}} p|_{y=h+0} + \dfrac{m_{\mathrm{h}}^{\mathrm{AlAs0.16Sb0.84}}}{m_{\mathrm{h}}^{\mathrm{InAs}}} e\upsilon_{\mathrm{pr}}^{\mathrm{InAs}} \exp\left(-\dfrac{\Delta E_{\mathrm{v}}}{k_{\mathrm{B}}T}\right) p|_{y=h-0}. \end{cases} \tag{s11}$$

Here, $m_{\mathrm{e}}^{\mathrm{InAs}}$ ($m_{\mathrm{e}}^{\mathrm{AlAs0.16Sb0.84}}$) and $m_{\mathrm{h}}^{\mathrm{InAs}}$ ($m_{\mathrm{h}}^{\mathrm{AlAs0.16Sb0.84}}$) are the effective electron and hole masses in InAs ($AlAs_{0.16}Sb_{0.84}$), $\varepsilon^{\mathrm{InAs}}$ and $\varepsilon^{\mathrm{AlAs0.16Sb0.84}}$ are the static dielectric constants of InAs and $AlAs_{0.16}Sb_{0.84}$, $\Delta E_{\mathrm{c}}$ ($\Delta E_{\mathrm{v}}$) is the difference in energy of the conduction (valence)-band edges in InAs and $AlAs_{0.16}Sb_{0.84}$. For simplicity, the back contact is modeled as an ideal Ohmic contact:

$$\begin{cases} \varphi|_{y=H-0} = V + \dfrac{k_{\mathrm{B}}T}{e} \ln\left(\dfrac{n_{\mathrm{eq}}^{\mathrm{AlAs0.16Sb0.84}}}{N_{\mathrm{c}}}\right), \\ n|_{y=H-0} = n_{\mathrm{eq}}^{\mathrm{AlAs0.16Sb0.84}}, \\ p|_{y=H-0} = p_{\mathrm{eq}}^{\mathrm{AlAs0.16Sb0.84}}, \end{cases} \tag{s12}$$

where $V$ is the bias voltage, $n_{\mathrm{eq}}^{\mathrm{AlAs0.16Sb0.84}}$ and $p_{\mathrm{eq}}^{\mathrm{AlAs0.16Sb0.84}}$ are the equilibrium electron and hole concentrations in $AlAs_{0.16}Sb_{0.84}$.

Finally, from the gain profile $g(y)$ obtained in the finite difference simulations, the net SPP gain $G$ is calculated using the power flow approach[3]:

$$\begin{aligned} G &= \frac{\int_{-w/2}^{w/2} dx \int_{0}^{h} g(y) S_z(x,y) dy}{\int_{-\infty}^{+\infty}\int_{-\infty}^{+\infty} S_z(x,y) dx dy} - \frac{\omega}{8\pi} \frac{\int_{-\infty}^{+\infty} dx \int_{-\infty}^{0} \mathrm{Im}\,\varepsilon_{\mathrm{Au}} |E|^2 dy}{\int_{-\infty}^{+\infty}\int_{-\infty}^{+\infty} S_z(x,y) dx dy} - W_{\mathrm{rad}} \\ &= \frac{\int_{-w/2}^{w/2} dx \int_{0}^{h} g(y) S_z(x,y) dy}{\int_{-\infty}^{+\infty}\int_{-\infty}^{+\infty} S_z(x,y) dx dy} - 2\,\mathrm{Im}\,\tilde{\beta}, \end{aligned} \tag{s13}$$

where $\varepsilon_{\mathrm{Au}}$ is the dielectric function of Au, $E$ is the SPP electric field, $g$ is the local optical gain, $W_{\mathrm{rad}}$ represents SPP radiation losses and $\tilde{\beta}$ is the complex SPP wavevector calculated neglecting band-to-band transitions in InAs.

**Calculation of the dielectric function of gold**

Dielectric function of gold was calculated in the infrared using the Drude model

$$\varepsilon_{\mathrm{Au}}(\omega) = 1 - \frac{\omega_{\mathrm{p}}^2}{\omega^2 + i\Gamma\omega}, \tag{s14}$$

where $\omega_{\mathrm{p}}$ is the plasma frequency and $\Gamma$ is the damping frequency. The plasma frequency is practically temperature-independent[10,11] and in gold is equal to[12-14] $1.37\times10^{16}$ s$^{-1}$. In the infrared, $\Gamma$ can be represented as the sum of four terms:

$$\Gamma = \gamma_{\mathrm{p}} + \gamma_{\mathrm{e}} + \gamma_{\mathrm{g}} + \gamma_{\mathrm{s}}. \tag{s15}$$

In the above expression, $\gamma_{\mathrm{p}}$, $\gamma_{\mathrm{e}}$, $\gamma_{\mathrm{g}}$ and $\gamma_{\mathrm{s}}$ are related to the electron-phonon, electron-electron, grain-boundary and surface scattering, respectively. The electron-phonon collision frequency $\gamma_{\mathrm{p}}$ is temperature-dependent[15]:

$$\gamma_{\mathrm{p}}(T) = \gamma_{\mathrm{p}}(300\ \mathrm{K})\frac{\frac{2}{5} + 4\left(\frac{T}{\theta}\right)^5 \int_0^{\frac{\theta}{T}} \frac{z^4}{\exp(z)-1}dz}{\frac{2}{5} + 4\left(\frac{300}{\theta}\right)^5 \int_0^{\frac{\theta}{300}} \frac{z^4}{\exp(z)-1}dz}, \tag{s16}$$

where $\theta$=170 K is the Debye temperature of Au. The electron-phonon collision frequency can be also related to the electron mean free path $\Lambda$ as $\gamma_{\mathrm{p}} \approx \upsilon_{\mathrm{F}}/\Lambda$, where $\upsilon_{\mathrm{F}}$ is the Fermi velocity in gold ($1.4\times10^8$ cm/s). At room temperature, $\Lambda$=38 nm and, consequently, $\gamma_{\mathrm{p}}(300\ \mathrm{K}) \approx 3.7\times10^{13}$ s$^{-1}$. Electron-electron scattering is represented by the sum of the temperature dependent and the frequency dependent terms[10]:

$$\gamma_{\mathrm{e}} = \gamma_{\mathrm{e}}^{\mathrm{T}}(T) + \gamma_{\mathrm{e}}^{\mathrm{f}}(\omega), \tag{s17}$$

where $\gamma_{\mathrm{e}}^{\mathrm{T}}(T)$ is much less than $\gamma_{\mathrm{p}}$ and is neglected in our calculations, while $\gamma_{\mathrm{e}}^{\mathrm{f}}(\omega)$ is expressed as[16]

$$\gamma_{\mathrm{e}}^{\mathrm{f}}(\omega) = \frac{\omega^2}{4\pi^2\omega_{\mathrm{p}}}. \tag{s18}$$

Surface scattering rate $\gamma_{\mathrm{s}}$ is determined by the thickness of the metal film $h$ and is given by[17]

$$\gamma_{\mathrm{s}} = \gamma_{\mathrm{p}}\left\{\left[1 - \left(\frac{3}{2\frac{h}{\Lambda}}\right)(1-p)\int_1^{\infty}\left(\frac{1}{t^3} - \frac{1}{t^5}\right)\frac{1-\exp\left(-\frac{h}{\Lambda}t\right)}{1-p\exp\left(-\frac{h}{\Lambda}t\right)}\mathrm{d}t\right]^{-1} - 1\right\}, \tag{s19}$$

where $p$ is the fraction of elastically scattered electrons (assumed to be zero in our calculations) and $h$ is the film thickness. Grain-boundary scattering arises from the fact that the gold film is polycrystalline. It can drastically alter the damping frequency $\Gamma$ and significantly increase Joule heating losses in the metal

if the grain size becomes comparable with the electron mean free path.[18] According to the theory of Mayadas et al.,[19] grain-boundary scattering rate $\gamma_g$ is expressed as follows:

$$\gamma_g = \gamma_p \left\{ \left[ 1 - \frac{3}{2}\alpha + 3\alpha^2 - 3\alpha^3 \ln\left(1 + \frac{1}{\alpha}\right) \right]^{-1} - 1 \right\}, \tag{s20}$$

where

$$\alpha = \frac{\Lambda}{D}\frac{R}{1-R}. \tag{s21}$$

Here, $D$ is the grain size, which strongly depends on the film thickness and the fabrication process, and $R$ is the grain-boundary reflection coefficient, which is approximately equal to 0.4 in the case of Au.[20]

To verify our model, we compare it with the experimental value of Johnson and Christy[14] for the damping frequency in the Drude formula. According to the data listed in the above reference, we took $h$=40 nm and determined the grain size as 30 nm (see Ref. 21). Substituting these values into Eqs. (s15-s21), we obtain the damping frequency in the range from $9.8\times10^{13}$ s$^{-1}$ (at $\hbar\omega$=0.64 eV) to $10.6\times10^{13}$ s$^{-1}$ (at $\hbar\omega$=1.5 eV), which is in a good agreement with the experimental result of Johnson and Christy[14] $\Gamma = (10.8 \pm 1.0)\times10^{13}$ s$^{-1}$.

Now, we apply the model to the calculation of the dielectric function of gold in the spectral range under consideration (0.34-0.44 eV). Assuming the gold film thickness to be about 100 nm and the corresponding grain size be equal to 60 nm (according to Ref. 21), we can easily calculate scattering contributions at room temperature: $\gamma_p = 3.7\times10^{13}$ s$^{-1}$, $\gamma_e = 6.6\times10^{11}$ s$^{-1}$ (at 392.5 meV), $\gamma_s = 6.0\times10^{12}$ s$^{-1}$, $\gamma_g = 2.2\times10^{13}$ s$^{-1}$,– and obtain $\Gamma = 6.6\times10^{13}$ s$^{-1}$ (at 392.5 meV). At 77 K, the electron-phonon collision frequency decreases down to $\gamma_p = 1.2\times10^{13}$ s$^{-1}$, whereas the surface scattering rate and the grain scattering rate do not change significantly ($\gamma_s = 6.5\times10^{12}$ s$^{-1}$, $\gamma_g = 2.1\times10^{13}$ s$^{-1}$) and $\gamma_e$ remains the same. Summing all the contributions, we get $\Gamma = 4.1\times10^{13}$ s$^{-1}$ at 392.5 meV. To calculate the damping frequency over the entire considered spectral range, we derive the explicit expression $\Gamma = \left[4.01 + 0.43(\hbar\omega)^2\right]\times10^{13}$ s$^{-1}$, where $\hbar\omega$ is measured in eV.

**Simulation of the SPP transmission through a 90-degree bend**

Transmission through a 90-degrees waveguide bend is simulated using the full-vectorial 3D finite element method (FEM). As a first step, the eigenmode electromagnetic problem is solved at a waveguide cross-section and the $TM_{00}$ mode is identified. Then, the field distribution corresponding to this mode is set as a source boundary condition (marked by a red rectangular in Figure S2(a)) in the 3D simulations. The validity of the 3D simulations is confirmed by modeling a straight waveguide. It is

found that the mode propagates with essentially the same characteristics as predicted by the eigenmode simulations.

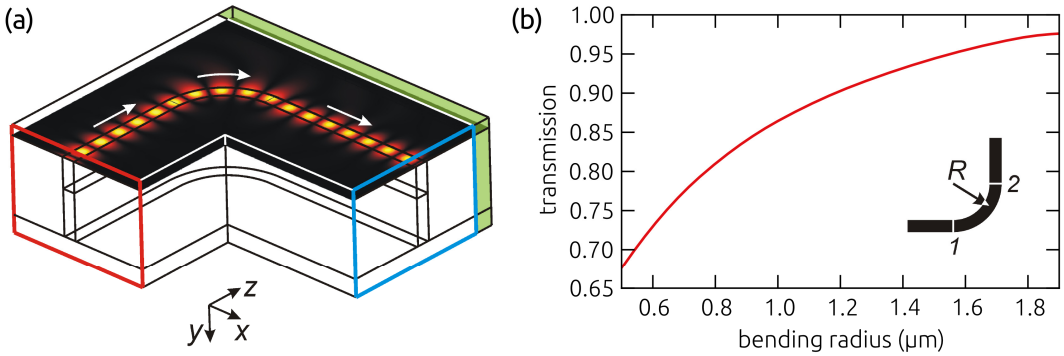


**Figure S2.** (a) Field map $\left|\mathrm{Re}\,E_y\right|$ of mode transmission through a 90-degree waveguide bend for the case of 1.5 μm bending radius of the waveguide central axis. (b) Transmission through the bend (curved interval between cross-sections *1* and *2* shown in the insert) as a function of the bending radius under electrical pumping providing full loss compensation in the case of a straight waveguide.

Dependence of the bend transmission on the bending radius is presented in Figure S2(b). It is calculated as a ratio of the power flow integrals over the waveguide core at the output (marked by a blue rectangular in Figure S2(a)) and at the input (marked by a red rectangular in Figure S2(a)). The actual lengths of the input and the output straight waveguide sections used in the 3D simulations (cut in the figure) were equal to 10 μm in order to allow the mode to settle after excitation at the source boundary and after transmission through the waveguide bend. The mode transmission is normalized to exclude the straight waveguide sections and is calculated for the case of full loss compensation in a straight waveguide. Perfectly matched layer (PML), marked by green in Figure S2(a), is placed at the outer boundary to absorb the radiation escaped from the bend (essential at smaller radii $R$<1 μm), which could (being partly reflected) affect the transmission results.

As shown in the Figure S2(b), the plasmonic mode can be transferred with 95% efficiency through a 90-degree bend having just 1.5 μm radius. The field map corresponding to this case is presented in Figure S2(a). As one can easily see, there is virtually no radiation losses from the waveguide, which was additionally checked using power flow integration over the boundary at which the PML is placed. Such small bending radius ultimately defines a very small (subwavelength) size of all circuit components, such as splitters, ring resonators etc.

**References**

(1) Snowden, C.M. *Introduction to Semiconductor Device Modelling*, World Scientific: Singapore, 1998.

(2) Sze, S.M. *Physics of Semiconductor Devices*, Wiley: New York, 1981.

(3) Fedyanin, D.Yu. Toward an electrically pumped spaser *Opt. Lett.* **2012**, *37*, 404-406.

(4) Casey, H.C.; Panish, M.B. *Heterostructure Lasers*, *Part A*, Academic: New York, 1978.

(5) Stern, F. Band-tail model for optical absorption and for the mobility edge in amorphous silicon *Phys. Rev. B* **1971**, *3*, 2636.

(6) Casey, H.C.; Stern, F. Concentration-dependent absorption and spontaneous emission on heavily doped GaAs *J. Appl. Phys.* **1976**, *47*, 631.

(7) Rhoderic, E.H. *Metal Semiconductor Contacts*, Clarendon Press: Oxford, 1978.

(8) Horio, K.; Yanai, H. Numerical modeling of heterojunctions including the thermionic emission mechanism at the heterojunction interface *IEEE Trans. on Electron Devices* **1990**, *37*, 1093-1098.

(9) Lopez-Gonzalez, J.M.; Prat, L. Numerical modelling of abrupt InP/InGaAs HBTs *Solid-St. Electron* **1996**, *39*, 523-527.

(10) Parkins, G.R.; Lawrence, W.E.; Christy, R.W. Intraband optical conductivity σ(ω,T) of Cu, Ag, and Au: Contribution from electron-electron scattering *Phys. Rev. B* **1981**, *23*, 6408-6416.

(11) Bouillard, J.-S. G.; Dickson, W.; O'Connor, D.P.; Wurtz, G.A.; Zayats, A.V. Low-temperature plasmonics of metallic nanostructures *Nano Lett*. **2012**, *12*, 1561-1565.

(12) Ordal, M.A.; Bell, R.J.; Alexander, R.W.; Long, L.L.; Querry M.R. Optical properties of Au, Ni, and Pb at submillimeter wavelengths *Appl. Opt.* **1987**, *26*, 744-752.

(13) Ordal, M.A.; Long, L.L.; Bell, R.J.; Bell, S.E.; Bell, R.R.; Alexander, R.W.; Ward, C.A. Optical properties of the metals Al, Co, Cu, Au, Fe, Pb, Ni, Pd, Pt, Ag, Ti, and W in the infrared and far infrared *Appl. Opt.* **1983**, *22*, 1099-1120.

(14) Johnson, P.B.; Christy, R.W. Optical Constants of the Noble Metals *Phys. Rev. B* **1972**, *6*, 4370-4379.

(15) Tillin, M.D.; Sambles, J.R. Phonon assisted absorption in thin Ag films using surface plasmon-polaritons *J. Phys.: Condens. Matter* **1990**, *2*, 7055.

(16) Aspnes, D.E.; Kinsbron, E.; Bacon, D.D. Optical properties of Au: Sample effects *Phys. Rev. B* **1980**, *21*, 3290-3299.

(17) Sondheimer, E.H. The mean free path of electrons in metals *Adv. Phys.* **1952**, *1*, 1.

(18) Chen, K.-P.; Drachev, V.P.; Borneman, J.D.; Kildishev, A.V.; Shalaev V.M. Drude Relaxation Rate in Grained Gold Nanoantennas *Nano Lett.* **2010**, *10*, 916-922.

(19) Mayadas, A.F.; Shatzkes, M.; Janak, J.F. Electrical resistivity model for polycrystalline films: the case of specular reflection at external surfaces *Appl. Phys. Lett.* **1969**, *14*, 345.

(20) Zhu, Y.F.; Lang, X.Y.; Zheng W.T.; Jiang, Q. Electron Scattering and Electrical Conductance in Polycrystalline Metallic Films and Wires: Impact of Grain Boundary Scattering Related to Melting Point *ACS Nano* **2010**, *4*, 3781-3788.

(21) Zhang, X.; Song, X.; Zhang, X.-G.; Zhang, D. Grain boundary resistivities of polycrystalline Au films *EPL* **2011**, *96*, 17010.